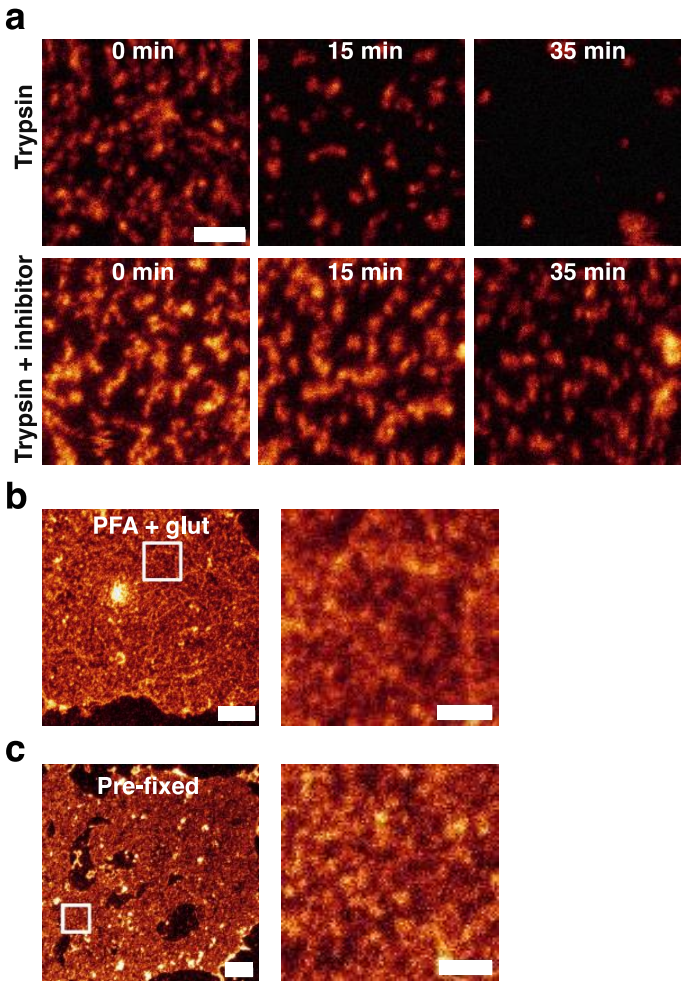

Supplementary Figure 1: Click-labelling reveals protein assemblies in unfixed membrane sheets, as well as in membrane sheets fixed using different protocols.

(a) Fluorescent assemblies visible in STED microscopy of unfixed membrane sheets are composed of proteins. STED images of click-labelled, unfixed PC12 membrane sheets treated with 1 mg/mL trypsin or with 1 mg/mL trypsin and 2 mg/mL trypsin inhibitor (shown in upper or lower panels, respectively) at RT. STED images were taken just before the addition of trypsin or trypsin + inhibitor (0 min), and at 15 and 35 min after the addition. Images of different membranes are shown to avoid photobleaching. Image intensity is scaled identically for all frames. Scale bar, 750 nm. **(b-c)** Different fixation protocols. We used paraformaldehyde (PFA) fixation to reveal protein assemblies in membrane sheets in Figure 3. We performed the same labelling here after a harsher fixation step, with 4% PFA and 0.2%

glutaraldehyde for 45 min at RT[1]. The right panel shows a high-zoom view of the area marked with the white square. **(c)** Alternatively, the sonication procedure was performed after fixation of PC12 cells with 4% PFA and 0.2% glutaraldehyde for 45 min. The sheets obtained in this experiment thus reflect the status of the membrane before sonication. A similar protein assembly pattern is observed. For panels **b** and **c** scale bars are 2 μm (left) and 500 nm (right).

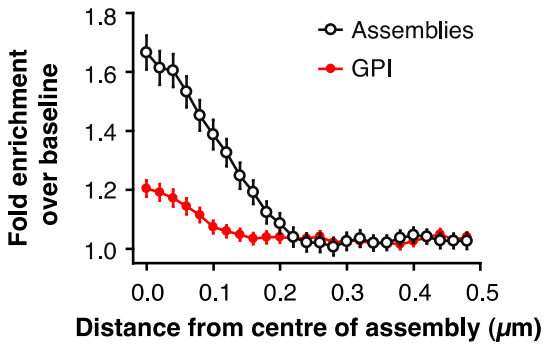

Supplementary Figure 2: Probing distribution of GPI-anchored proteins with respect to the protein assemblies.

For investigating the distribution of GPI anchored proteins versus protein assemblies, ACP with a GPI anchor signal sequence was expressed in AHA-labelled COS-7 cells, and was coupled to Atto647N through an ACP-synthase reaction on living cells, before sonication. After sonication, fixation and click reaction, membranes were imaged by two-colour STED microscopy. The graph shows the averaged line scans, normalized to the baseline (mean ± SEM, n=600 protein assemblies).

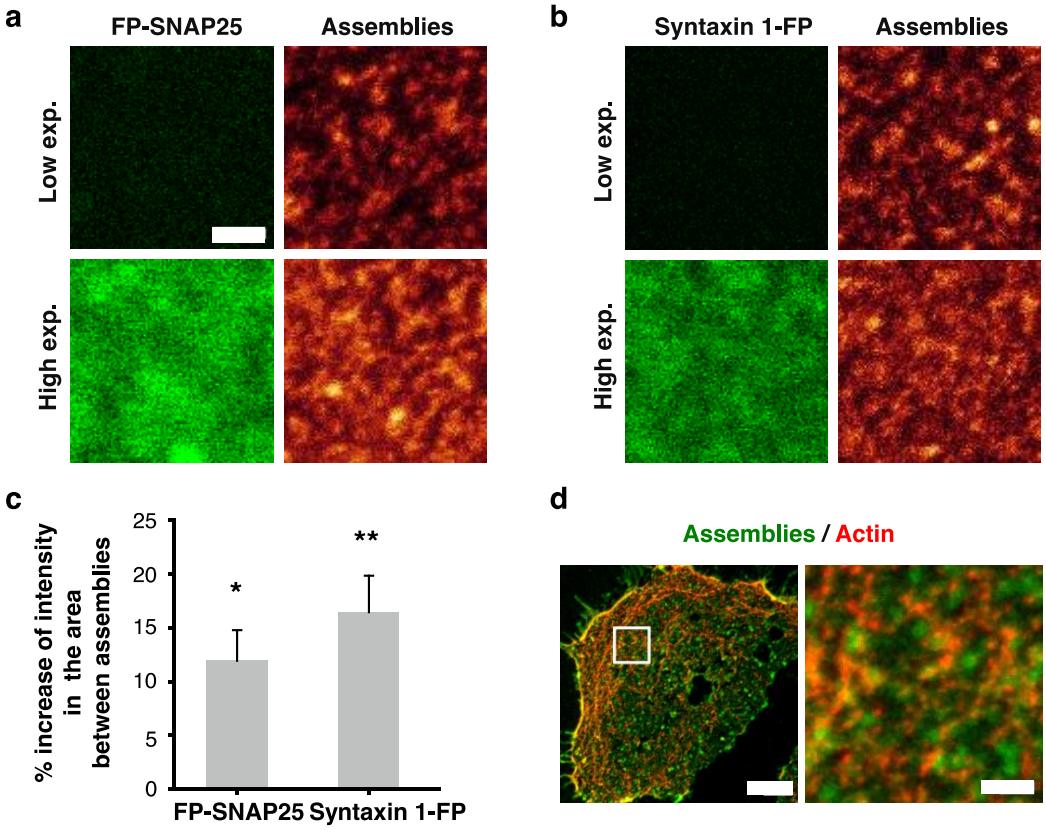

Supplementary Figure 3: Effects of overexpression of proteins on the general protein organization. Actin organization on membrane sheets.

(a-b) SNAP25 and syntaxin 1 were tagged with fluorescent proteins (FP) and overexpressed in PC12 cells. The left column displays the fluorescent protein signal (confocal images). The protein distribution, revealed by click labelling, is shown on the right (STED images). Image intensities are scaled identically. Scale bar, 500 nm. Top panels: membranes expressing low levels of FP-SNAP25 or syntaxin 1-FP, respectively. Bottom panels: membranes expressing high levels of the fluorescently tagged proteins. **(c)** The graph quantifies the increase in fluorescence intensity in the area between assemblies, as percentage of the control, non-overexpressing membranes. The graph indicates mean ± SEM; n=18-37 sheets per condition, from two independent experiments, P = 0.0206 (*, $p<0.05$) for SNAP25 and $p=0.00469$ for syntaxin 1 (**, $p<0.01$), t-tests. According to Jarque-Bera tests, the data were not different from samples with normal distributions ($p>0.05$). The variance was similar for all groups (0.41 to 0.47). **(d)** Two-colour STED images of immunostaining for actin (red) on PC12

membrane sheets (immediately fixed with 4% PFA after sonication). Protein assemblies labelled by click reaction are shown in green. The image on the right is the high-zoom view of the area marked with the white rectangle in the overview image. Scale bars are 4 μm and 750 nm, respectively. Note the abundance of the actin staining on isolated sheets and more favourable localization of actin at the edges of the green assemblies.

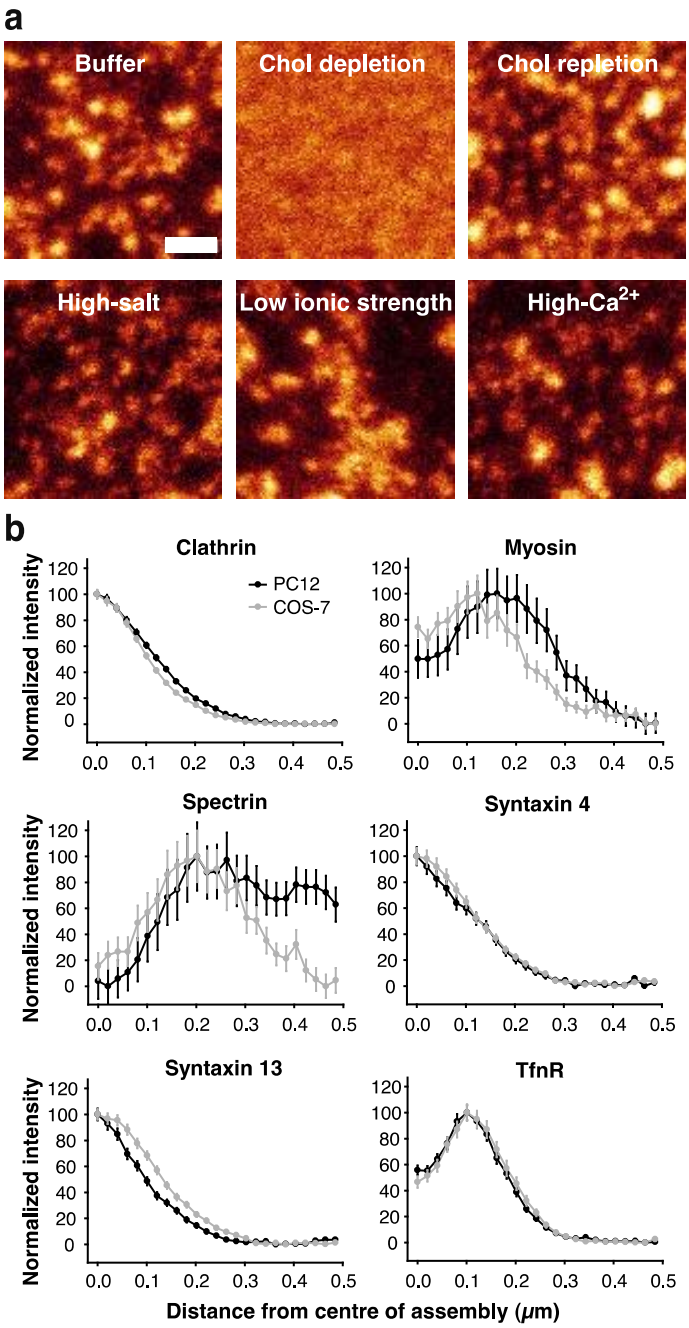

Supplementary Figure 4: Similar phenotypes and distributions observed in COS-7 membrane sheets.

(a) The panels show STED images of membrane sheets from COS-7 cells treated as for the PC12 cells in Figures 5a and 6a. Briefly, the membrane sheets were incubated at 37°C with sonication buffer (15 min), or subjected to cholesterol depletion with MBCD (5 mM, 5 min, followed by incubation in sonication buffer for 10 min). To replete cholesterol, after treatment with MBCD (5 mM, 5 min), cholesterol was loaded by applying MBCD-cholesterol (right; 5

mM, 10 min, at 37 °C). Alternatively, the ionic manipulations in Figure 5a were applied by 20 min incubation of the COS-7 membrane sheets at 37°C with sonication buffer (not shown, similar to the buffer condition in top left image) as control or with high-salt buffer (containing 0.5 mM KCl), low ionic strength buffer (320 mM sucrose, 5 mM HEPES-KOH), or high-calcium buffer (containing 1 mM Ca^{2+}), for 20 min. Scale bar, 500 nm. Note that the phenotypes are similar to those observed for PC12 membranes: relatively minor effects of all treatments, with the exception of cholesterol depletion. As in PC12 membranes, cholesterol repletion recovers protein assemblies. **(b)** Specific proteins were fluorescently labelled through immunostaining (red) on PFA-fixed COS-7 plasma membranes. The graphs indicate normalized averaged line scans, as for the PC12 cells in Figure 7 (mean ± SEM, n=385-550 protein assemblies). For comparison purposes, line scans of the same proteins in PC12 membranes (from Fig. 7) were also plotted. All of the proteins were distributed in the same fashion as in PC12 membranes.

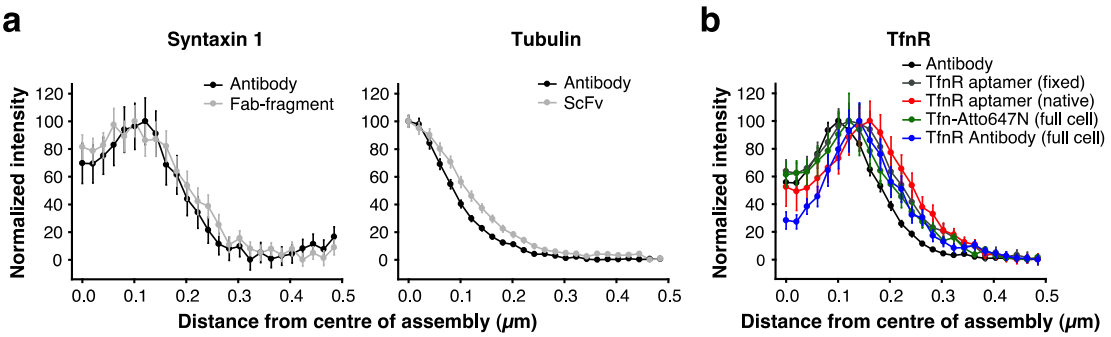

Supplementary Figure 5: Control stainings with different types of probes and with different sample preparation conditions.

(a) Line scans obtained for PC12 membranes as in Figure 7, using monovalent directly labelled probes such as Atto647N-conjugated anti-syntaxin 1 Fab fragment, and anti-tubulin single chain variable fragment (scFv), instead of conventional antibodies (mean ± SEM, n=276-308 protein assemblies). For comparison purposes, the traces obtained with antibodies, from Figure 7, are also plotted (black). **(b)** Analysis of TfnR staining under different conditions. Immunostaining: TfnR was either probed with an antibody against a cytosolic epitope on membrane sheets (from Fig. 7) or with another antibody against a surface epitope on full cells fixed with 4% PFA + 0.2% glutaraldehyde. For the latter, the cells were labelled by click chemistry and were embedded in plastic resin. In order to be able to focus at the membrane surface with a z-resolution comparable to that in membrane sheets, ultrathin sections (<20 nm) were cut as described in Supplementary Methods and two-colour STED imaging was then performed. In a separate experiment, living cells were labelled with Atto647N-conjugated transferrin (Tfn) followed by fixation, click reaction, plastic embedding and sectioning. Alternatively, a TfnR aptamer conjugated to Atto647N was applied to the living PC12 cells, prior to sonication, and the proteins were labelled by click chemistry, either after fixation or on unfixed membranes. The graph shows the baseline and peak normalized average line scans for all conditions (mean ± SEM, n=184-549 protein assemblies). Note that the distribution of TfnR was similar in all labelling and membrane manipulation conditions.

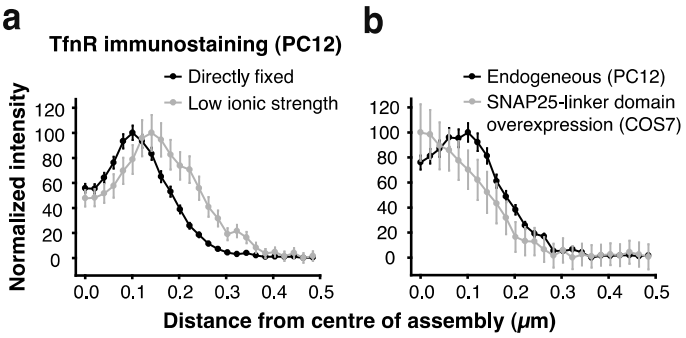

Supplementary Figure 6: Additional controls regarding the distributions of membrane proteins

(a) Averaged normalized line scans (mean ± SEM, n=493 protein assemblies). obtained by immunostaining of PC12 membrane sheets for the transferrin receptor (TfnR) after a 20-min incubation with low ionic strength buffer, which causes the formation of larger protein assemblies (Fig. 5a,e). For comparison, the line scan for the TfnR immunostaining from Fig. 7 is also plotted (black). Note that TfnR is still enriched at the edges of the larger assemblies. **(b)** The truncated version of SNAP25, lacking the SNARE domains and coupled to GFP (thus consisting of GFP coupled to the palmitoylated linker domain of SNAP25) was overexpressed in COS-7 cells where its main interaction partners are not expressed, and was detected by a GFP antibody. The graph shows the averaged line scans (mean ± SEM, n=1280 protein assemblies, from 2 independent experiments), as in panel **a**. Note that this fragment distributes to protein assembly centres, different from the endogenous SNAP25 distribution in PC12 cells (from Fig. 7).

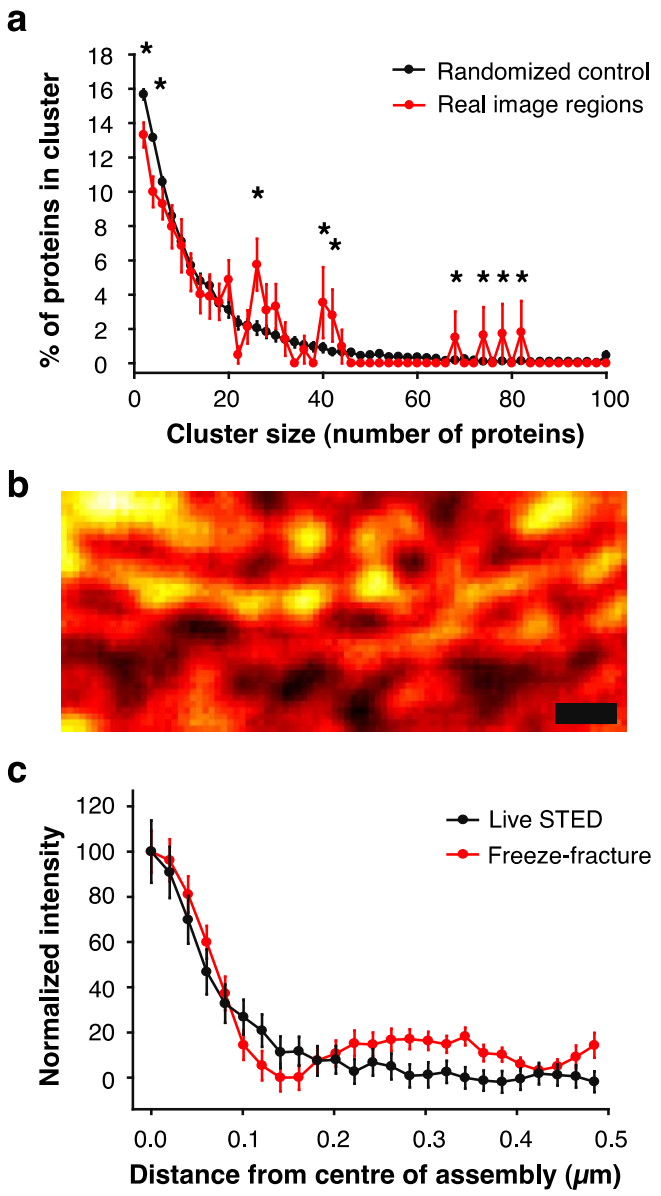

Supplementary Figure 7: Interpretation of protein distribution in freeze-fracture electron microscopy images.

(a) We have analysed the distribution of intramembrane particles (representing membrane proteins) in several images (from Figure 7 in Heuser et al., 1979, Figure 3 in Heuser and Reese 1981, and Figure 1 in Miller and Heuser, 1984) obtained via freeze-fracture by Heuser and Reese in the past[2-4]. We used the Matlab function clusterdata to assign the particles to different clusters, based on the distances to their neighbours. The graph shows the percentage of the proteins found in clusters of specific sizes (red). We performed the same analysis on images in which the protein positions were randomized (black). Values that were significantly

different from the randomized control are marked by an asterisk (*, Wilcoxon rank sum test, at 5% significance level, n=18 regions from 3 images). The analysis suggests that several cluster sizes appear in the membranes at higher rates than expected from random positioning. **(b)** To compare the electron microscopy distribution of intramembrane particles with the distribution of fluorescently labelled proteins (Figs. 1b and 3a), we replaced the intramembrane particles in Figure 7 of Heuser et al., 1979[2] with fluorescent molecules *in silico*, and convolved the images with a measured STED point-spread-function (PSF) to obtain a fluorescence-like image. Scale bar, 200 nm. Protein patterns similar to those from Figures 1b and 3a are obvious. **(c)** For a quantitative comparison, we performed line scans as in Fig. 7b, on *in silico* generated fluorescence images from Figure 7 of Heuser et al., 1979 and Figure 3 of Heuser and Reese 1981[2,3], and also on our live cell STED images of AHA-labelled COS-7 cells, as in Figure 1b. The graph shows the averaged line scans (mean ± SEM, n=43 spots for freeze-fracture images and n=1195 spots, from 3 independent repetitions for live cell STED imaging of protein assemblies).

For panel **a** we used the Wilcoxon rank test, which tests whether the numbers in two vectors are independent samples from continuous distributions with the same medians, since it does not require the two vectors to have the same lengths, and does not require the values to be normally distributed. The mean variances of the two curves were similar (9.13 and 8.57 for the experimental data and the random control, respectively).

Supplementary Tables

Protein name	Membrane association	Post-translational anchor	Localization	General function	Enrich-ment in assemb-lies	Cent-reness
Actin	Cytoskeletal		Cytoplasm / cell cortex	Cytoskeletal element	1.77	0.49
APP	Bitopic Integral	Palmitoylation (2 sites, occurs rarely)[5]	Endomemb-rane system	Cell surface receptor of neurons	4.31	1.51
BACE	Bitopic Integral	Palmitoylation (4 sites)[6]	Endomemb-rane system	Proteolytic processing of the amyloid precursor protein (APP)	4.00	0.66
Bassoon	Peripheral	N-terminal myristoylation	Cytoplasm / transport vesicles / cell membrane	Organization of the cytomatrix at the active zone	2.35	0.51
α-N-catenin	Peripheral		Cell membrane / cytoplasm	Linker between cadherin adhesion receptors and the cytoskeleton, to regulate	6.65	1.77

				cell-cell adhesion		
Caveolin 1	Monotopic integral	Palmitoylation (3 sites)	Cell membrane	Caveolae formation	3.24	1.08
Clathrin heavy chain	Peripheral		Cytoplasm / vesicles / cell membrane	Major coat component of coated pits and vesicles	10.77	1.48
Cortactin	Cytoskeletal		Cytoplasm / cell cortex	Cytoskeletal element	8.00	1.29
Dynamin 1,2,3	Peripheral		Cytoplasm / vesicles/ cell membrane	Vesicular trafficking, fission	2.36	0.58
ERM	Peripheral		Cell membrane/ cell cortex	Connection of cytoskeletal elements (actin) to the plasma membrane	2.14	0.53
Flotillin 2	Peripheral	N-terminal myristoylation and palmitoylation (3 sites)[7]	Cell membrane / endosomes	Scaffolding protein within caveolar membranes	2.01	0.93
Munc18-1	Peripheral		Cell membrane / cytoplasm	Regulation of synaptic vesicle docking and fusion	2.31	0.82

Myosin Va	Cytoskeletal		Cytoplasm	Cytoskeletal element	1.62	0.62
NSF	Peripheral		Cytoplasm	SNARE-complex disassembly, chaperone	3.79	1.38
α-SNAP	Peripheral		Cytoplasm	SNARE-complex disassembly	4.50	1.22
SNAP23	Monotopic integral	Palmitoylation (5 sites)	Cell membrane	SNARE (fusion) molecule; part of the constitutive secretion machinery	2.52	0.88
SNAP25	Monotopic integral	Palmitoylation (4 sites)	Cell membrane	SNARE (fusion) molecule; part of the neurotransmit-ter release machinery	3.46	0.64
β-Spectrin II	Cytoskeletal		Cytoplasm / cell cortex	Cytoskeletal element	1.36	0.62
Synaptophy-sin	Polytopic Integral (four-pass)		Secretory vesicles	Structural component of synaptic	1.41	0.63

				vesicles and dense-core vesicles		
Syntaxin 1	Bitopic Integral		Cell membrane	SNARE (fusion) molecule; part of the neurotransmitter release machinery	1.87	0.61
Syntaxin 13	Bitopic Integral		Endomembrane system	SNARE (fusion) molecule; part of the endosomal fusion machinery	4.30	1.29
Syntaxin 4	Bitopic Integral		Plasma membrane	SNARE (fusion) molecule; part of the constitutive secretion machinery	3.10	1.11
TfnR	Bitopic Integral	Palmitoylation (2 sites)	Cell membrane / endosomes	Receptor for transferrin; cellular uptake of iron	6.88	0.50

α-Tubulin	Cytoskeletal		Cytoplasm	Cytoskeletal element (microtubules)	8.77	1.62

Supplementary Table 1. Summary of all specific proteins investigated.

The proteins are described according to the protein database Uniprot, www.uniprot.org, and to references therein. The membrane association is classified as follows:

Monotopic integral proteins: permanently attached to the membrane from only one side.

Bitopic integral proteins: have segments at both sides of the lipid bilayer, and are permanently attached to it via one transmembrane domain.

Polytopic integral proteins: span the lipid bilayer more than once, and are permanently attached to it via several transmembrane domains.

Peripheral proteins: temporarily associated with the lipid bilayer through interactions with lipids or membrane proteins.

Cytoskeletal proteins: soluble elements of cortical cytoskeleton.

Centreness was determined as follows, from the line scans drawn over immunostained protein assemblies in Figure 7b. We measured the ratio between the intensity of specific proteins and that of the protein assemblies, at two points: 1) the centre of the assembly (Specific Protein $\text{intensity}_{\text{centre}}$/Protein Assembly $\text{intensity}_{\text{centre}}$), and 2) the half-width point, representing the edge (Specific Protein $\text{intensity}_{\text{edge}}$/Protein Assembly $\text{intensity}_{\text{edge}}$). Centreness was then obtained by dividing the first ratio (from the centre) by the second one (from the edge). This parameter is equal to 1 for proteins that are randomly distributed within the assemblies, is higher than 1 for proteins that are enriched in the centre, and is lower than 1 for proteins that prefer the edges.

Supplementary Methods

Reagents. Trypsin inhibitor (Type I-P) and trypsin from bovine pancreas were purchased from Sigma-Aldrich. BSA (Albumin – Fraction V) was purchased from Applichem. The sources of other reagents are given in Methods and Supplementary Methods sections where the respective protocols are described.

Antibodies. Following the click reaction, immunostainings were performed with 1:50-1:200 dilutions of the following primary antibodies: anti-pan-actin (mouse monoclonal, Norvus, NB 600-535), anti-APP (rabbit polyclonal, Synaptic Systems, 127-002), anti-BACE (rabbit polyclonal, Santa Cruz, Sc10748), anti-bassoon (rabbit polyclonal, Synaptic Systems, 141002), anti-α-N-catenin (rabbit polyclonal, Cell Signaling, 2131), anti-caveolin 1 (rabbit monoclonal, Abcam, ab2910), anti-clathrin heavy chain (mouse monoclonal, BD Biosciences, 10499), anti-cortactin (mouse monoclonal, Synaptic Systems, 313-111), anti-dynamin 1,2,3 (BD Biosciences, 610245), anti-phospho-ezrin (Thr567) / radixin (Thr564) / moesin (Thr558) (rabbit monoclonal, Cell Signaling, 3149), anti-flotillin 2 (mouse monoclonal, Santa Cruz), anti-GFP (mouse monoclonal, Invitrogen, A-11120), anti-munc 18-1 (rabbit polyclonal, Synaptic Systems, 116-002), anti-myosin Va (rabbit polyclonal, Sigma-Aldrich, M5062), anti-NSF (rabbit polyclonal, Synaptic Systems, 123-002), anti-PIP2 (mouse monoclonal, Abcam, ab11039), anti-α-SNAP (mouse monoclonal, Synaptic Systems, 112-111), anti-SNAP23 (rabbit polyclonal, Synaptic Systems, 112-202), anti-SNAP25 (mouse monoclonal, Synaptic Systems, 111-011), anti-β-spectrin II (mouse monoclonal, BD Biosciences, 612 562), anti-syntaxin 1 (mouse monoclonal, Synaptic Systems, 110-001), Atto647N-coupled anti-syntaxin 1 (mouse monoclonal Fab fragment, Synaptic Systems, 110-011), anti-syntaxin 4 (rabbit polyclonal, Synaptic Systems, 110-042), anti-syntaxin 13 (rabbit polyclonal, Synaptic Systems, 110-133), anti-TfnR cytoplasmic domain (mouse monoclonal, Invitrogen,

13-6800), anti-α-tubulin (rabbit polyclonal, Synaptic Systems, 302-203), and Atto647N-coupled anti-α/β-tubulin single chain Fv fragment (scFv[8]). An exception was made for flotillin2 and PIP2 antibodies, which were applied onto sheets for 15 min prior to fixation. Secondary antibody stainings were performed with Atto647N-coupled anti-rabbit-IgG (Sigma, 40839) or Star635-coupled anti-mouse-IgG (Abberior, 2-0002-002-0) antibodies. For imaging, the STED setup detailed in Methods was used in two-colour mode.

Synthesis and characterization of Chol-PEG-KK114 and Chol-PEG-Atto490LS. To synthesize a cholesterol analogue containing photostable fluorescent dyes suitable for STED-microscopy, we used a strategy which improved the partitioning of other lipid analogues dramatically[9]. Namely, we put a long water-soluble PEG linker between the membrane probe and the dye, which keeps the dye in the water phase. Chol-PEG(3400)-KK114 (or Atto490LS) was prepared from 1 μmol of Chol-PEG(3400)-amine in 0.2 mL of dry N,N-dimethylformamide, 20 μL (0.15 mmol) of triethylamine and 1 μmol of KK114 NHS (or Atto490LS NHS) ester. The product was isolated by elution with a chloroform:methanol:water mixture (70:25:3). For characterization, lipid phase partitioning was checked in giant unilamellar vesicles (GUVs). GUVs were prepared by swelling dried lipid films deposited on low melting point agarose[10]. Briefly, 100 μl of a pre-heated 1% agarose solution was spin-coated (3000 rpm) on cleaned microscopy cover glass. After spin-coating, the agarose was dried by heating the cover glasses to 40°C for 30 min on a heating plate. After drying, 30 μl of a 5 g/L lipid solution (Dioleoyl phosphatidylcholine (DOPC) / brain sphingomyelin / cholesterol, 2:2:1[11], dissolved in methanol / chloroform, 1:1) was spin-coated (3000 rpm) on top of the agarose and residual solvent was removed by applying vacuum for 20 min. Finally, the dried lipid film was hydrated in pure water at 50°C for 5 min, and then slowly cooled to RT. The lipid mixture contained 0.01 mol% of Chol-PEG-KK114 (Chol-PEG-tto490LS) and DiO. To estimate the partitioning of Chol-PEG-KK114

(Atto490LS) between the Ld and the Lo phase, GUVs were imaged at the equatorial plane and the distribution of DiO was used to identify phases. Lo partitioning was calculated to be 51% according to Lo% = $intensity_{Lo}$ / ($intensity_{Lo}$ + $intensity_{Ld}$). Partitioning of the PEGylated cholesterol probe was independent of the respective fluorescent dye (KK114 or Atto490LS).

Knockdown and overexpression constructs. Syntaxin 1 and SNAP 25 knockdowns (Fig. 5b) were performed using siRNAs. For SNAP25, 3 different siRNAs targeting:
5'-GTTGGATGAGCAAGGCGAA-3' [12],
GGATGAGCAAGGCGAACAA and
TAATATAGGGTTTGTCGAA sequences for both SNAP25 isoforms were designed.
For syntaxin 1, 5 different siRNAs were designed with target sequences:
5'-CACCAAAGGTCTCGGTAC-3',
TTAAGAAGACAGCGAACA,
GGTCCAAGTTGAAAGCGAT,
GGAGGTAATGACCGAATAT, and
GCTAAAGAGCATCGAGCAG.
The small interfering RNAs (siRNAs) were purchased from Thermo Scientific Dharmacon as 2'-deprotected duplexes and resuspended in RNase-free solutions according to the manufacturer's instructions. PC12 cells were transfected with cocktails of these siRNAs using Lipofectamine 2000 (Invitrogen) 72 h (in parallel to AHA incubation) before sonication.

For overexpression experiments (Supplementary Fig. 3a-c), PC12 cells were transfected using Lipofectamine 2000 (Invitrogen) with syntaxin1-pHluorin (in pEGFP-N1 starting vector from Clontech, EFGP was replaced with pHluorin as described in the past[13]) and YFP-SNAP25b (in pYFP-C1, Clontech, the construct was previously described in Zilly et al., 2011[14]). Alternatively, COS-7 cells were transfected with a GFP-fused SNAP25 construct lacking both

SNARE motifs (GFP-SNAP25 linker domain, Supplementary Fig. 6b), as previously described[15]. COS-7 cells were transfected with GPI-anchor signal sequence fused with ACP (GPI-ACP) and tagged with Atto647N (Supplementary Fig. 2) through ACP-synthase reaction as previously described[16]. Transfections were performed during the second day of the AHA incubation, and cells were allowed to express the proteins for 48 h in presence of AHA.

Organelles. PC12 post-nuclear supernatants (PNS) were produced as described previously[17]. For studying mitochondria, the PNS fractions were centrifuged (at 2665 g, for 1 h at 4°C) onto BSA-coated coverslips. The coverslips were incubated in sonication buffer with 5 mM cholesterol-MBCD complex[18] for 30 min at 37°C, to load cholesterol into their membranes (or in sonication buffer alone, as control). The samples were then washed, fixed with 4% PFA, coupled to fluorescent dyes by click reactions, and immunostained against the cytosolic mitochondrial epitope TOMM20 (using mouse anti-TOMM20, Sigma, WH0009804M1) to identify specifically the mitochondria. For studying endosomes, early endosomal (EE) fractions were enriched from freshly prepared PNS by sucrose gradient centrifugations as described before[19]. After, centrifugation onto coverslips as above, EE fractions were depleted of cholesterol by incubation with 45 mM MBCD, for 30 min at 37°C, followed by washing, fixation and click reaction. Controls were incubated with buffer alone.

Labelling whole cells from extracellular side. PC12 cells were incubated in Ringer buffer on ice for 1 h transferrin conjugated to Atto647N. The cells were later sonicated to obtain membrane sheets and were then fixed and labelled by click reactions. Alternatively, whole cell immunostainings were performed as by applying anti-TfnR primary antibody targeting the extracellular domain (mouse monoclonal, Abcam, Ab1086) from extracellular side onto whole PC12 cells fixed with 4% PFA and 0.2% glutaraldehyde. This step was followed by thorough washing, and application of secondary antibodies, as for the immunostaining of

membrane sheets. For the whole cell experiment (Supplementary Fig. 5b), fluorescently labelled fixed cells were embedded in plastic resin and sectioned as indicated below under "Plastic embedding".

Plastic embedding. For Supplementary Figure 5b, whole cells were fixed and labelled by click chemistry as above. They were then embedded in 2,4,6-Tris[bis(methoxymethyl)amino]-1,3,5-triazine, as described in the past[13]. This was followed by thin-section processing using an EM UC6 ultramicrotome (Leica), again as previously described[13]. Sections of 10-20 nm were used in STED imaging.

Labelling with the TfnR aptamer. An Atto647N-coupled TfnR aptamer (sequence published before[20]) was prepared as previously described[21]. Fresh before use, it was folded by heating in a thermocycler to 75°C (for 3 min in PBS containing 5 mM $MgCl_2$), followed by cooling to 20°C at a rate of 1°C/min. PC12 cells were incubated for 20 min on ice with a final dilution of 400 nM of the folded aptamer in Ringer buffer (124 mM NaCl, 5 mM KCl, 2 mM $CaCl_2$, 1 mM $MgCl_2$, 30 mM D-glucose and 25 mM HEPES, pH 7.4) containing 1 µg/mL salmon sperm DNA as a blocking reagent. The cells were then washed with Ringer buffer and sonicated. Membrane sheets were labelled with Chromeo494 through click reactions either directly after sonication (unfixed) or after fixation (with 4% PFA for 20 min on ice, and for 30 min at RT) and quenching. The unfixed sheets were washed and imaged in K-Glu buffer immediately after preparation, whereas the fixed membranes were embedded in Mowiol before imaging.

Data analysis. All analyses were performed with the help of Matlab software (The Mathworks Inc.), using self-written routines.

Figure 2f. We performed 1.23 µm-long line scans (3 pixel, or 61 nm, wide) over the protein assemblies, centred on the assemblies of the dominant colour (i.e., centred on the AHA assemblies in the AHA-dominated side of the membrane sheets). From the line scans, we determined the fold enrichment (peak versus baseline) both in the dominant colour and in the subordinate colour. For the 60 min condition, it was not possible to determine which colour is dominant. Therefore same regions of interest were analysed twice and normalized either to green or red signal. The ratio between these enrichment values is shown in Figure 2f.

Figures 3b. Protein assemblies were identified as the areas whose intensity was above the background intensity (selected on empty coverslip areas). For accurate identification, images were first filtered using median and averaging filtering. Rectangular regions of interest were selected, and the pixels whose fluorescence intensity was clearly above the background staining intensity were identified (within more than two standard deviations from the mean background intensity; the background was selected on empty coverslip areas adjacent to the membrane sheets). This procedure generated masks for each individual assembly. Size identification was performed automatically by fitting Lorentzian curves to the mask areas and determining the full-width-at-half-maximum (FWHM). For non-circular structures, the largest diameter was taken as the size value.

Figures 4a-d, 7b and Supplementary Figures 2, 4, 5, 6 and 7: Line scans (1.23 µm in length, 3 pixels in width) were performed manually on protein assemblies and were subsequently averaged. The line scans were centred on the midpoints of protein assemblies, on the raw data images. All curves were normalized to the baseline signal, obtained from the average line scans (the region flanking the peaks). Typically 30-50 line scans were obtained from one membrane sheet. For analysis line scans were pooled from several membrane sheets, from up to 4 independent experiments. We would like to point out that the fold enrichment of the

proteins over the baseline (given in Fig. 4b-d, for example) is an underestimate, since the baseline region obtained by these measurements (lateral to the peak) includes signal from a considerable proportion of large protein assemblies, whose assembly areas overlapped with the baseline bordering the more frequent small assemblies.

Figure 5d: For a simple indication of protein clustering on the plasma membrane, we calculated the total space occupied by all of the protein assemblies, expressed as percentage of the total membrane area. This measurement, termed "area occupied by assemblies" in the figures, is insensitive to changes in the structure of protein assemblies, but reports accurately any changes in the relative proportions of assemblies and protein-poor areas. The images were analysed exactly as for Figure 3b, and the total area occupied by the assemblies was measured.

Figure 5e. Apparent diameters for assemblies were found as described above for Figure 3b. The average two-dimensional assembly sizes were computed by assuming a circular geometry for the assemblies, and calculating the resulting circular surface.

Figure 6a: To find the "protein-poor area" we performed the same analysis as for Figure 5d, but here we refer to the area of the membrane sheets that was within the range of background staining rather than the area occupied by assemblies. As above, all values are presented as percentage of control.

Figure 6b: Protein clustering in organelles was determined as follows: line scans of 1-pixel width and variable length were drawn manually along the membranes of the organelles, and the coefficient of variation of the intensity along the line scan (standard deviation divided by the mean) was calculated. This value is a direct indication of protein assemblies, since it

reports the magnitude of the differences between the peak signals (assemblies) and the baseline. For display, images were deconvolved with Huygens Essential software (Scientific Volume Imaging), using the inbuilt routines (applying classical maximum likelihood estimation algorithm) designed specifically for STED images.

Supplementary Figure 3c: The protein assemblies and the areas outside of protein assemblies were determined as for Figure 3b. Protein intensity in each category was then automatically detected for all regions of interest within one image, and region values were averaged to obtain representative data.

Supplementary References

1. Tanaka, K. A. K. *et al.* Membrane molecules mobile even after chemical fixation. *Nat Methods* **7,** 865–866 (2010).
2. Heuser, J. E. *et al.* Synaptic vesicle exocytosis captured by quick freezing and correlated with quantal transmitter release. *J Cell Biol* **81,** 275–300 (1979).
3. Heuser, J. E. & Reese, T. S. Structural changes after transmitter release at the frog neuromuscular junction. *J Cell Biol* **88,** 564–580 (1981).
4. Miller, T. M. & Heuser, J. E. Endocytosis of synaptic vesicle membrane at the frog neuromuscular junction. *J Cell Biol* **98,** 685–698 (1984).
5. Bhattacharyya, R., Barren, C. & Kovacs, D. M. Palmitoylation of amyloid precursor protein regulates amyloidogenic processing in lipid rafts. *J Neurosci* **33,** 11169–11183 (2013).
6. Vetrivel, K. S. *et al.* Alzheimer disease Abeta production in the absence of S-palmitoylation-dependent targeting of BACE1 to lipid rafts. *J Biol Chem* **284,** 3793–3803 (2009).
7. Neumann-Giesen, C. *et al.* Membrane and raft association of reggie-1/flotillin-2: role of myristoylation, palmitoylation and oligomerization and induction of filopodia by overexpression. *Biochem J* **378,** 509 (2004).
8. Nizak, C. *et al.* Recombinant antibodies against subcellular fractions used to track endogenous Golgi protein dynamics in vivo. *Traffic* **4,** 739–753 (2003).
9. Honigmann, A., Veronika, M., Hell, S. & Eggeling, C. STED microscopy detects and quantifies liquid phase separation in lipid membranes using a new far-red emitting fluorescent phosphoglycerolipid analogue. *Faraday Discuss* **161,** 77–89 (2013).
10. Horger, K. S., Estes, D. J., Capone, R. & Mayer, M. Films of Agarose Enable Rapid Formation of Giant Liposomes in Solutions of Physiologic Ionic Strength. *J Am Chem*

Soc **131,** 1810–1819 (2009).
11. Veatch, S. L. & Keller, S. L. Seeing spots: complex phase behavior in simple membranes. *BBA-Mol Cell Res* **1746,** 172–185 (2005).
12. Cahill, A. L., Herring, B. E. & Fox, A. P. Stable silencing of SNAP-25 in PC12 cells by RNA interference. *BMC Neurosci* **7,** 9 (2006).
13. Hoopmann, P. *et al.* Endosomal sorting of readily releasable synaptic vesicles. *Proc Natl Acad Sci USA* **107,** 19055–19060 (2010).
14. Zilly, F. E. *et al.* Ca2+ induces clustering of membrane proteins in the plasma membrane via electrostatic interactions. *EMBO J* **30,** 1209–1220 (2011).
15. Halemani, N. D., Bethani, I., Rizzoli, S. O. & Lang, T. Structure and Dynamics of a Two-Helix SNARE Complex in Live Cells. *Traffic* **11,** 394–404 (2010).
16. Eggeling, C. *et al.* Direct observation of the nanoscale dynamics of membrane lipids in a living cell. *Nature* **457,** 1159–1162 (2009).
17. Barysch, S. V., Jahn, R. & Rizzoli, S. O. A fluorescence-based in vitro assay for investigating early endosome dynamics. *Nat Protoc* **5,** 1127–1137 (2010).
18. Christian, A., Haynes, M. & Phillips, M. Use of cyclodextrins for manipulating cellular cholesterol content. *J Lipid Res* **38,** 2264–2272 (1997).
19. Bethani, I. *et al.* Endosomal Fusion upon SNARE Knockdown is Maintained by Residual SNARE Activity and Enhanced Docking. *Traffic* **10,** 1543–1559 (2009).
20. Wilner, S. E. *et al.* An RNA alternative to human transferrin: a new tool for targeting human cells. *Mol Ther Nucleic Acids* **1,** e21 (2012).
21. Opazo, F. *et al.* Aptamers as potential tools for super-resolution microscopy. *Nat Methods* **9,** 938–939 (2012).